Solubility Considerations for Cloud Condensation Nuclei (CCN) Activity Analysis of Pure and Mixed Black Carbon Species

Kanishk Gohil[a], *Reese Barrett*[a], *Dewansh Rastogi*[a], *Chun-Ning Mao*[a], *Qi Yao*[a], *Akua Asa-Awuku*[a*]

[a]Department of Chemical and Biomolecular Engineering, University of Maryland, College Park, MD 20742 USA

*Correspondence – Akua Asa-Awuku (asaawuku@umd.edu) +3014058527

Keywords: Carbonaceous aerosols, Black Carbon (BC), CCN activity, Hygroscopicity, Aerosol indirect effect

Abstract

Black Carbon (BC) is an aerosol that is released into the atmosphere due to the incomplete burning of biomass and can affect the climate directly or indirectly. BC commonly mixes with other primary or secondary aerosols to undergo aging, thereby changing its radiative properties and cloud condensation nuclei (CCN) activity. The composition of aged BC species in the atmosphere is difficult to measure with high confidence and so their associated CCN activity can be uncertain. In this work, the CCN activity analysis of BC is performed using laboratory measurements of

proxy aged BC species. Vulcan® XC72R Carbon Black was used as the representative of BC, and 3 structural isomers of benzenedicarboxylic acid – phthalic acid (PTA), isophthalic acid (IPTA) and terephthalic acid (TPTA) – were mixed with BC to generate 3 different proxies of aged BC species. Most studies related to CCN activity analysis BC aerosol use the traditional Köhler Theory or an adsorption theory (such as the Frenkel-Halsey-Hill Adsorption Theory). PTA, IPTA and TPTA fall in the sparingly water-soluble range and therefore do not fully obey either of the aforementioned theories. Consequently, a novel hybrid activity model (HAM) was used for the CCN activity analysis of the BC mixtures studied in this work. HAM combines the features of adsorption theory via the adsorption isotherm with the features of Köhler Theory by incorporating solubility partitioning. The results in this work show that HAM improves the representation of CCN activity of pure and mixed BC aerosol species with high certainty; evident from a generally better goodness of fit, $R^2 > 0.9$. This work implies that the hygroscopicity parameterization based on HAM captures the size-dependent variability in the CCN activity of the pure and aged BC species.

Introduction

Black carbon (BC) aerosol is significant due to its effect on the atmosphere and climate. This is a result of the observed effects of BC on air quality, climate change, and human welfare [1–3]. BC is produced from incomplete biomass and fossil fuel combustion and is one of the main biomass burning tracers in the atmosphere alongside other primary and secondary organic aerosols (POAs and SOAs) [4,5]. BC is the second most important contributor to the warming of the climate after carbon dioxide [6,7]. However, BC aerosols may also significantly indirectly affect the climate via

interactions with clouds. The aerosol-indirect effect of pure and coated BC aerosols must be well understood to better understand their climate forcing.

Carbonaceous aerosols, and BC aerosol particularly, have complex molecular level interactions with water [8–10]. BC particles in the atmosphere exist as agglomerates or nodules and conglomerates with other species; BC are rarely observed in pure form and are known to age downwind of emission sources [11]. Aging can alter BC morphology, BC oxidation state and the aged particles ranging from a few nm to several μm in size, may contain co-condensed phases [12,13]. Aged BC can internally or externally mix with other aerosols present in the atmosphere [7]. The pure and mixed, or aged BC are known to act as Cloud Condensation Nuclei (CCN) under supersaturated ambient conditions and can therefore affect the climate "indirectly" through altering cloud properties [9,14–16]. CCN activation is traditionally described using Köhler theory and works well for highly water-soluble solutes. However, due to the strong water insoluble nature of BC, traditional Köhler theory should not be applied to study BC CCN activity and droplet growth.

For insoluble aerosols such as BC, CCN activity and water uptake are aptly described via the effect of water vapor adsorption on the particle surface [17–19]. Adsorption activation theory combines adsorption isotherms and curvature effects to describe insoluble aerosol droplet growth. Frenkel-Halsey-Hill adsorption theory (FHH-AT) is formulated by combining the FHH isotherm with the Kelvin effect [20] and is the most widely used CCN activity theory for the droplet growth of insoluble wettable aerosols [18,19,21–28]. Additionally, the FHH isotherm has been combined with Köhler Theory for the CCN activity analysis of insoluble particles coated with soluble species assuming a "core-shell" morphology. Kumar et al. (2011 a, b) also described CCN activation of mineral dust species containing a soluble salt fraction using the combination of the classical Köhler and FHH adsorption theories. Other studies have developed frameworks to theoretically describe

CCN activity of insoluble aerosols using multilayer adsorption models accounting for the curvature and contact angle of the droplets [19].

There exists several published work for which BC is present in atmospheric aerosol with organic and inorganic material [29–31]. However, the explicit treatment of low-solubility organic mixtures with black carbon is missing. So far, the CCN activity studies of BC particles under supersaturated or subsaturated conditions predominantly focus on BC mixed with readily water-soluble species. One such compound is NaCl (observed as a component of sea salt); Dusek et al, (2006) performed chamber CCN measurements and showed a significant enhancement in the CCN activity of BC particles on mixing with 5% NaCl. Zhang et al. (2004) observed that BC particles aged with sulfuric acid showed up to ~10-fold and ~2-fold enhancement in their scattering and adsorption properties, after undergoing hygroscopic growth at 80% relative humidity. Dalirian et al., (2018) performed CCN analysis of BC particles coated with various water soluble and insoluble organic compounds using the core-shell CCN model. Dalirian found that water-soluble coating with glutaric and levoglucosan organic could be predicted. However, the CCN activity of BC with other water-insoluble materials like oleic acid, could not be explained by the size affect alone. Other studies include CCN analysis of ambient BC aged with high hygroscopicity sea spray aerosols [32].

This work studies the water uptake and droplet formation of particles composed of effectively water-insoluble organics mixed with BC using controlled laboratory compounds and measurements. Vulcan® was chosen as the representative of graphitic and water insoluble BC aerosol. Vulcan is a synthetic commercially available BC substance that possess high electrical conductivity and is widely used for electrocatalytic applications [33]. Three low water solubility structural isomers of benzene di-carboxylic acid – Phthalic acid (PTA), Isophthalic acid (IPTA)

and Terephthalic acid (TPTA) – were mixed with BC. PTA, IPTA and TPTA are prominent benzene polycarboxylic acids detected in the atmosphere [34–41]. PTA, IPTA and TPTA are produced from biomass burning and emissions of automobile exhaust [42–46]. PTA and its isomers are known tracers of benzanthracene, naphthalene-1 and methylnaphthalene-1 [47–49] and are likely co-emitted with soot so BC mixtures with these oxygenated aromatic acids can be considered proxies for aged soot.

Recently a hybrid activity model (HAM) was developed to model the water-uptake and hygroscopicity of effectively water-insoluble aerosol[50]. HAM combines solubility partitioning with the FHH adsorption isotherm to describe the droplet growth. HAM suggests that the hygroscopicity is size dependent. HAM was found to be effective with sparingly soluble organic aerosol – however, its utility with relevant atmospherically mixed insoluble species (BC, mineral dust, nanopolymers etc.) has yet to be tested. In this manuscript, HAM is applied and used to describe the variability in the water uptake behavior of BC particles mixed with low solubility water solubility compounds (PTA, IPTA and TPTA). Additionally, Transmission Electron Microscopy (TEM) captures images of mixed aerosol to identify particle morphology that may affect water uptake behavior. The compounds and their mixtures considered in this work are useful because they could represent atmospheric organic aerosol composition. The CCN activity measurements of pure and mixed BC particles also provide an efficient means to further validate the application of the newly developed HAM. In the following sections, we first describe the experimental setup to obtain experimental CCN activation data for pure and mixed BC. We then briefly describe FHH-AT and HAM models and compare predictions to data and discuss the results in the context of aged soot particles, droplet growth, and cloud formation.

Methodology

Chemicals and Sample Preparation – Pure BC and Internal Mixtures with Aromatic Acid Aerosols (AAAs)

Vulcan® (Cabot Vulcan® XC72R Carbon Black) was used as the representative of black carbon (BC). Vulcan® has been extensively studied used as a proxy for black carbon [51–56], and was used to analyze soot mixtures in this work. Phthalic acid (PTA, 1,2 – benzenedicarboxylic acid, >99.5%, Sigma-Aldrich®) and terephthalic acid (TPTA, 1,4 – benzenedicarboxylic acid, 98%, Sigma-Aldrich®) and Isophthalic acid (IPTA, 1,3 – benzenedicarboxylic acid, >99%, Fisher Scientific®) were aromatic acid aerosols (AAAs) used in this study. The physical properties of BC and AAAs are summarized in Table 1. AAA compounds were mixed with BC in a 1:1 mass ratio. The water uptake behavior of the 3 AAA compounds in this study have been previously described in detail in Gohil et al. (2022). The mass-to-volume concentration of the pure BC solution was 72 mg BC in 200 ml ultrapure water (Milli-Q or Millipore®, 18.2MΩ cm^{-1}). The mass-to-volume concentration of BC-to-AAA internal mixtures was also 72 mg (36 mg BC was mixed with 36 mg of AAA) in 200 ml ultrapure water (Milli-Q or Millipore®, 18.2MΩ cm^{-1}). Furthermore, the acidity of the pure AAA aerosol and 1:1 BC-to-AAA aerosol was quantified with their pH. The pH of PTA, IPTA and TPTA was found to be 5.24, 5.43 and 5.94, respectively. Low acidity suggests that the AAA samples are not strong organic solvents. However, BC can dissolve in stronger acidic solutions [57]; therefore, the weak organic acid solutions here have minimal dissolution of BC in AAA. Before preparing all the pure and internally mixed BC aerosol, dry Vulcan® was first heated at 450 °C for 6 hours. The pure and internally mixed aqueous suspensions of BC were then sonicated in a 30 °C water bath for 9 hours. The BC aerosol was sonicated in a 20 °C water bath during all aerosol measurements; including the CCN, shape factor and TEM grid experiments as described in detail below.

Table 1. Physical and chemical properties of BC and AAA compounds.

Compounds	Molecular weight (M_s, g mol^{-1})	Density (ρ_s, g cm^{-3})	Solubility (C, m^3 m^{-3})
Black Carbon (Vulcan® XC72R)	12	~1.8	$< 10^{-6}$
Phthalic acid	166.14	1.59	3.77×10^{-3}
Isophthalic acid	166.14	1.53	7.84×10^{-5}
Terephthalic acid	166.13	1.52	1.12×10^{-5}

CCN Measurements

A continuous flow stream-wise thermal gradient Cloud Condensation Nuclei Counter (CCNC, Droplet Measurement Technologies (DMT) (Roberts & Nenes, 2005 - CCN 100) measured CCN of pure and internally mixed BC aerosol. The DMT CCNC is a widely used instrument for droplet growth measurements in supersaturated conditions[31,59–61] and only a brief description of experimental setup is provided here. Polydisperse aerosol was generated and dried from aqueous suspensions as described in the *Chemicals and Sample Preparation* section. An electrostatic classifier (DMA 3080) size selected monodisperse aerosol corresponding to a fixed electrical mobility diameter. The size-selected aerosols exiting the DMA were then split into two streams. One stream entered a condensation Particle Counter (CPC, TSI 3776) at 0.3 L min^{-1} to measure total dry particle concentration (C_{CN}), and a second stream entered the CCNC at 0.5 L min^{-1} and constant supersaturation to measure activated particle (droplet) counts (C_{CCN}). A sheath flow rate of 8 L min^{-1} was applied across the experimental setup to maintain a sheath-to-sample ratio of 10:1. The experiments were performed over a range of varying supersaturations from 0.2%-1.6%, with 0.1% step size. Each supersaturation was held constant for 15 minutes for every sample and particle size to provide sufficient time for the CCNC column temperature gradient, and hence the supersaturation to stabilize. This process of stepping through each particle size for a range of supersaturations is henceforth referred to as a "step-mode" process. Furthermore, CCNC supersaturations ranging between 0.2% and 1.6% were calibrated using ammonium sulfate

($(NH_4)_2SO_4$, AS) aerosol (Sigma-Aldrich®, >99.9%) prior to performing measurements for pure and mixed BC samples. AS data used for CCN calibration is provided in the supporting information (Section S1).

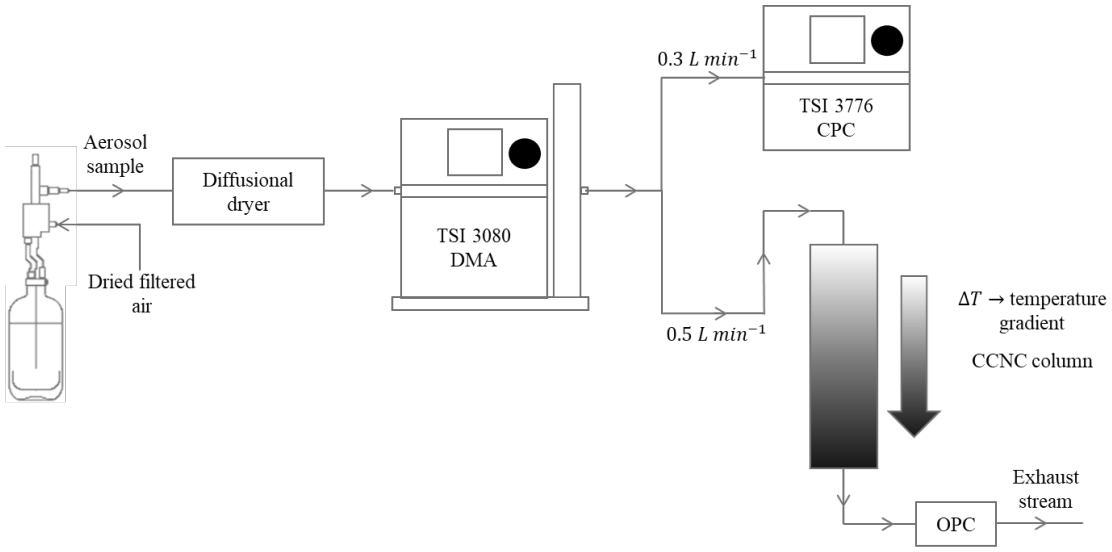

Fig. 1. Schematic of a CCN measurement experimental setup. The DMA and the CPC are operated in the stepping mode to obtain number concentrations at selected electrical mobility diameter.

Effective Density Estimation and Shape Factor Measurements

Dynamic shape factor and effective particle density are measured with an Aerodynamic Aerosol Classifier (AAC, Cambustion Ltd.), TSI DMA 3080 and TSI CPC 3776 connected in series. The AAC and DMA measure the aerodynamic and electrical mobility diameters of the particles, respectively. The application of the experimental setup has been examined extensively in the literature[62–65]. A brief description of the experimental setup and calibration is provided in this paper. Polydisperse aerosol was generated from aqueous suspensions as described above. The AAC selected monodisperse aerosol corresponding to an aerodynamic diameter (D_{ae}). The sample and the sheath flow rates were maintained at 0.3 L min^{-1} and 3.0 L min^{-1} respectively (i.e., sheath-to-sample flow ratio = 10:1). The monodisperse aerosol was then passed through the DMA and the CPC in series operating in the Scanning Mobility Particle Sizer (SMPS) mode to generate a

number size distribution with respect to the electrical mobility diameter. The median diameter of the distribution was considered as the approximate electrical mobility diameter (D_{mo}) corresponding to the initially set D_{ae}. The size-resolved effective density and dynamic shape factor of the pure and mixed aerosols were calculated to further obtain their respective volume equivalent diameters applied to CCN measurement (supporting information, Section S2).

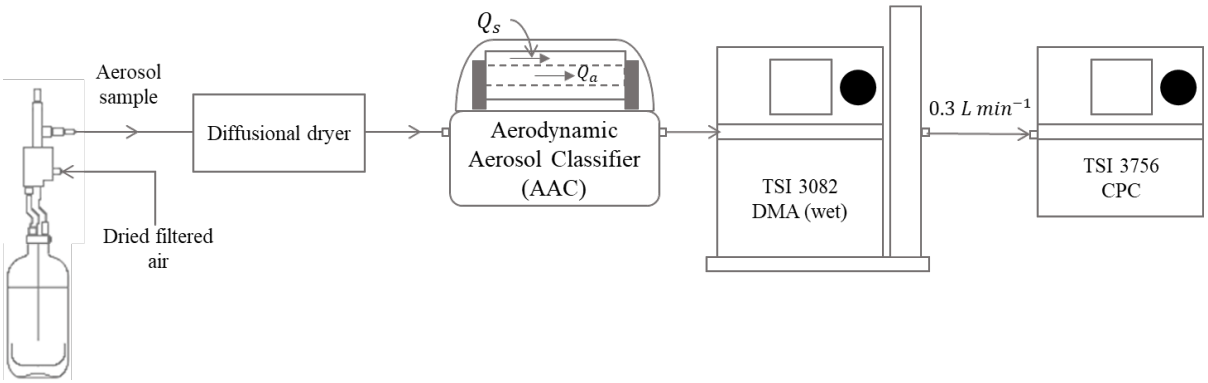

Fig. 2. Schematic of the shape factor and effective density experimental setup. The AAC selects dry aerosol with aerodynamic diameter (D_{ae}) and the SMPS measures a number size distribution of AAC-selected dry particles with electrical mobility diameters (D_{mo}).

CCN Activity Analysis – PyCAT

Python-based CCN Analysis Tool – PyCAT [65] was used to process, analyze, and visualize the calibration and BC data. PyCAT was developed for CCN analysis using scanning data collected using the DMA or AAC size selection experimental setup. In this study, a new module has been added to PyCAT to perform CCN analysis of step-mode data. The new module of PyCAT is capable of processing and analyzing data collected with respect to fixed electrical mobility diameter and varying CCNC supersaturations. Consequently, the activation ratio $\left(\frac{C_{CCN}}{C_{CN}}\right)$ of a given sample for a fixed dry diameter $\left(D_{dry}\right)$ are resolved by supersaturations (S). Following this, a sigmoidal function can be fit to the activation ratio as,

$$y = \frac{(A_1 - A_2)}{1 + e^{((x - x_0)/dx)}} - A_2 \qquad (1)$$

In Eq. (1), y is the dependent variable $\frac{C_{CCN}}{C_{CN}}$, A_1 and A_2 are the minimum and maximum of the sigmoid respectively, dx is the slope of the sigmoid, x_0 is the inflection point of the sigmoid (generally the midpoint of the sigmoid), and x is the independent variable (S). x_0 corresponds to the critical supersaturation (S_c) at the fixed dry diameter and is physically defined as the size at which 50% of all particles are activated. After size transformation, the volume equivalent diameters of the particles were implemented as their dry diameter $\left(D_{dry}\right)$.

Transmission Electron Microscopy (TEM)

Pure and mixed BC nano-sized particles were collected and analyzed with Transmission Electron Microscopy. The JEOL 2100 (TEM; LaB6 filament) was used in this work [66,67]. Specifically, aerosols pass through a neutralizer and the charged particles (Kr-85, TSI 3077A) were then deposited for 4 hours onto an electrically grounded lacey carbon-coated copper TEM grid (TED PELLA). The aerosols were charged using an aerosol neutralizer (Kr-85, TSI 3077A) and then passed through a wire mesh holding the TEM Grid at a sample flowrate of 0.3 lpm. The mesh and the grid were electrically grounded to ensure the particles deposited onto the grid adhered to the surface. Particle concentrations were then monitored using a CPC. Additional details of the grid deposition and measurement procedure are provided in Rastogi and Asa-Awuku (2022) [67]. For EDX and EELS analysis, the particles were deposited on a Silicon Nitride (SiN) grid. The deposited particles were then imaged at an accelerating voltage of 200 kV and a magnification range of 50-150 k. To minimize sample damage, the exposure time was limited to 90 sec.

Theory and Analysis

Frenkel-Halsey-Hill Adsorption Theory (FHH-AT)

The FHH-AT model describes droplet formation and growth via the adsorption of water on a particle surface. FHH-AT combines the FHH isotherm with the curvature effect (Kelvin term) to determine the water vapor over the droplet surface (supersaturation) during water uptake [20]. The FHH isotherm defines the water activity through adsorption of aqueous multilayers as a function of surface coverage (θ). The FHH isotherm is mathematically expressed as follows,

$$a_{w,FHH} = \exp(-A_{FHH}\theta^{-B_{FHH}}) \qquad (2)$$

The 2 empirical parameters (A_{FHH}, B_{FHH}) account for the surface and bulk contributions to droplet growth. A_{FHH} parameterizes the interactions between particle surface and the first adsorbed aqueous monolayer. B_{FHH} parameterizes the interactions between particle surface and the subsequently adsorbed aqueous monolayers. A_{FHH} and B_{FHH} respectively describe the amount of adsorbed water on particle surface as well as the radial distance away from the particle up to which the attractive forces can cause adsorption. In Eq. (2), $\theta = \frac{D_p - D_{core}}{2D_w}$, where D_p is the droplet diameter, D_{core} is the diameter of the insoluble core, and D_w is the diameter of a water molecule and has a value of 0.275 nm. Combining Eq. (2) with the curvature effect (Kelvin term), the FHH-AT can be expressed as,

$$S = a_{w,FHH} \exp\left(\frac{4\sigma_w M_w}{RT\rho_w D_p}\right) \qquad (3)$$

where σ_w, M_w and ρ_w are the surface tension, molecular weight, and density of water, respectively. R is the ideal gas constant and T is the temperature. It is important to note that the 2 empirical parameters are species dependent and can be determined by applying least square minimization on the maxima of FHH-AT equilibrium curve fitted to the experimental CCN activity measurements. The FHH-AT has previously been modified to incorporate different physical

properties of aerosol particles. One such modification is based on the inclusion of the contact angle of the adsorbed aqueous layers on the particle surface [18,19].

Hybrid Activity Model (HAM)

The hybrid activity model (HAM) incorporates solubility partitioning[50] with FHH-AT. The solubility partitioning transforms the ideal Raoult's law such that it includes the solubility of the compound (or, compounds) in the aerosol composition. With this approach, the effect of solid, undissolved core on droplet activation and water uptake can be included towards water uptake along with the contribution from dissolved particle within the aqueous phase. Moreover, the FHH empirical parameters (A_{FHH}, B_{FHH}) for each sample are the same computed by fitting the FHH-AT to the CCN activation data. The mathematical formulation of HAM is as follows,

$$S = a_{w,HAM} \exp\left(\frac{4\sigma_w M_w}{RT\rho_w D_p}\right) \qquad (4)$$

where $a_{w,HAM} = a_{w,Raoult} \cdot a_{w,FHH}$. $a_{w,Raoult}$ is the Raoult's law term which is defined as $\gamma_w X_w$, where γ_w is the activity coefficient and X_w is the mole fraction of water in the aqueous phase of the droplet. Considering the droplet to be infinitely dilute, $\gamma_w \approx 1$ and $a_{w,Raoult}$ can then be approximated as $X_w = \frac{n_w}{n_w + n_s}$, where n_w are the number of moles of water and n_s are the total number of moles of the solute(s) in the aqueous phase of the droplet.

Physically, the HAM water activity describes the droplet growth and water uptake process in 3 stages. Stage 1 is the start of the water uptake by adsorption on the particle surface followed by minute droplet growth. Since there in an infinitesimal amount of solute dissolved in the aqueous phase in stage 1, $X_w \approx 1$ and therefore $a_{w,HAM} \approx a_{w,FHH}$. In stage 2, a finite amount of solute continues to dissolve into the aqueous phase. Therefore, $a_{w,HAM} = X_w \cdot a_{w,FHH}$ in stage 2. X_w and $a_{w,FHH}$ vary continuously during the droplet growth in stage 2 and are estimated using the bulk

solubilities of each compound with the instantaneous droplet diameter and solute mass dissolved[50,68]. Stage 3 begins when the entire mass of the initial solute particle has dissolved into the aqueous phase with no undissolved solute left. In stage 3, the $a_{w,HAM} = X_w$ (Raoult's law). Additional details and description of the formulation of HAM is provided in Gohil et al. (2022).

Hygroscopicity Parameterization from FHH-AT and HAM

The single hygroscopicity parameter is denoted by κ and is mathematically formulated by relating it to the water activity of the CCN activity model. The general formulation for κ was provided by [69] and is expressed as follows,

$$\frac{1}{a_w} = 1 + \kappa \frac{V_s}{V_w} \qquad (5)$$

where a_w is the water activity term, V_s is the volume of the dry particle, and V_w is the volume of water in the aqueous phase. The κ parameter derived from a CCN model can be parameterized by substituting the a_w in Eq. (5). Following this procedure, the experimental and theoretical single hygroscopicity parameters for FHH-AT and HAM have been previously developed. The full derivation of the hygroscopicity parameterizations based on FHH-AT and HAM have been provided by Mao et al. (2022) and Gohil et al. (2022), respectively.

**Results and Discussion

The particles generated from BC and BC mixtures in this study have a range of non-uniform sizes and shapes (Figure 3). TEM images show that small BC particles can be spherical however can agglomerate to form larger sized particles. BC mixtures with aromatic acids can modify the shape of these particles. Thus size-resolved effective density and dynamic shape factor of pure and mixed BC particles must be calculated prior to CCN analysis. The dry electrical mobility diameters (D_{mo}) of the pure and mixed BC samples were converted to their corresponding volume equivalent diameters (D_{ve}) using in-situ measurements (supporting information, Section S2) prior to CCN

activity analysis. D_{ve} was determined for the CCN analysis with respect to every D_{mo}. D_{ve} are a better representation of particle sizes than the D_{mo}[65], especially for hygroscopicity parameterizations based on FHH-AT or HAM due to explicit dependence on particle sizes. Moreover, the average dynamic shape factor was found to be unique to each specific particle composition and chemical constituency. There was also a strong dependence observed on particle size (Section S2) which is visualized in the TEM images obtained for each sample. Generally, particles became spherical with an increase in D_{mo}.

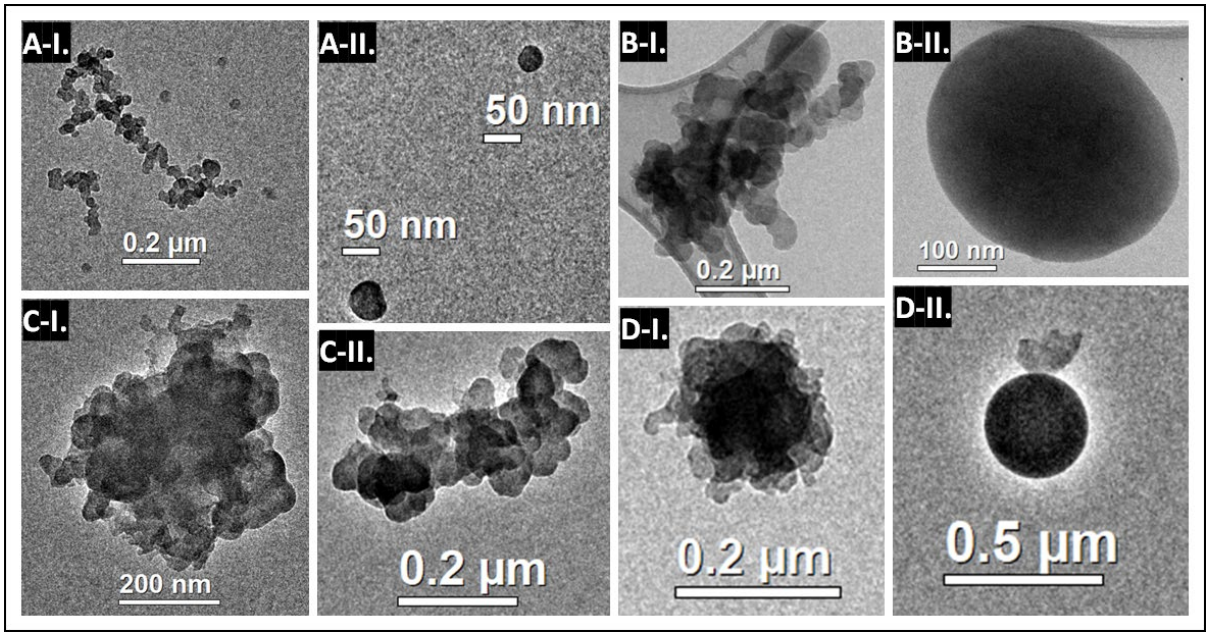

Fig. 3. TEM images of different sized particles of pure BC (A-I, AII) and BC mixed with Phthalic (B-I, B-II), Isophthalic (C-I, C-II) and Terephthalic (D-I, D-II) acid, respectively.

CCN Activity of Pure and Internally Mixed BC

CCN measurements of pure and mixed BC particles were performed. The CCN activity data of pure and mixed BC are summarized in detail in the supporting information (Section S3, Figure S3). For each sample, number concentrations were measured with respect to varying

supersaturations in the CCNC while the dry particle diameters were held fixed. The sigmoidal functions fitted to the activation ratio is also shown along with the critical supersaturations. The sigmoidal fits for mixed BC samples corresponding to each dry particle diameter consisted of a single plateau. The single plateau is indicative of a homogenous particle[65]. The assumption of internally mixed aerosol mixtures is also supported by Energy Dispersive X-ray (EDX) analysis results (Figure 4). Fig. 4 shows mixtures of BC with phthalic, isophthalic, and terephthalic acid species. For constant particle sizes, TEM and CCN analysis suggested that the mixtures presented here had components of carbon and oxidized species uniformly distributed throughout the particles, therefore forming homogenous internal mixtures.

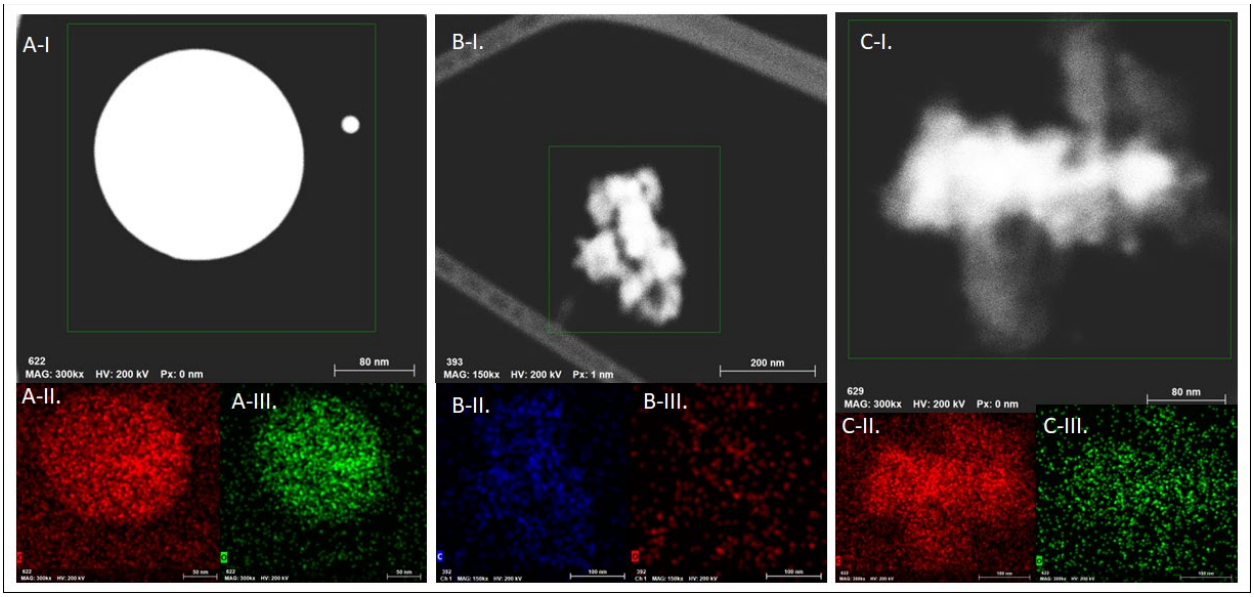

Fig. 4. Images show dark field images of BC mixtures with Phthalic (A-I), Isophthalic (B-I) and Terephthalic acid (C-I). Images II and III for each mixture are EDXs images showing relative distribution of carbon and oxygen respectively for each mixture.

The FHH-AT fits and CCN data of pure BC and mixed BC-AAA species were compared with the pure AAA samples (Figure 5). Fig. 5 shows the D_{ve} of the dry particles with respect to critical

supersaturations. The empirically determined FHH parameters for pure and mixed BC samples, with the FHH parameters of the pure AAA samples that were determined in [50] are summarized in Table 2. Mixed BC aerosol are less active than their pure aromatic acid CCN activity. Moreover, the CCN activity of the mixtures decreases in the same order as that of the corresponding pure AAAs. Also, the slope of the FHH-AT fits of mixed samples diverged away from the FHH-AT fits of the corresponding AAA with an increasing D_{ve}.

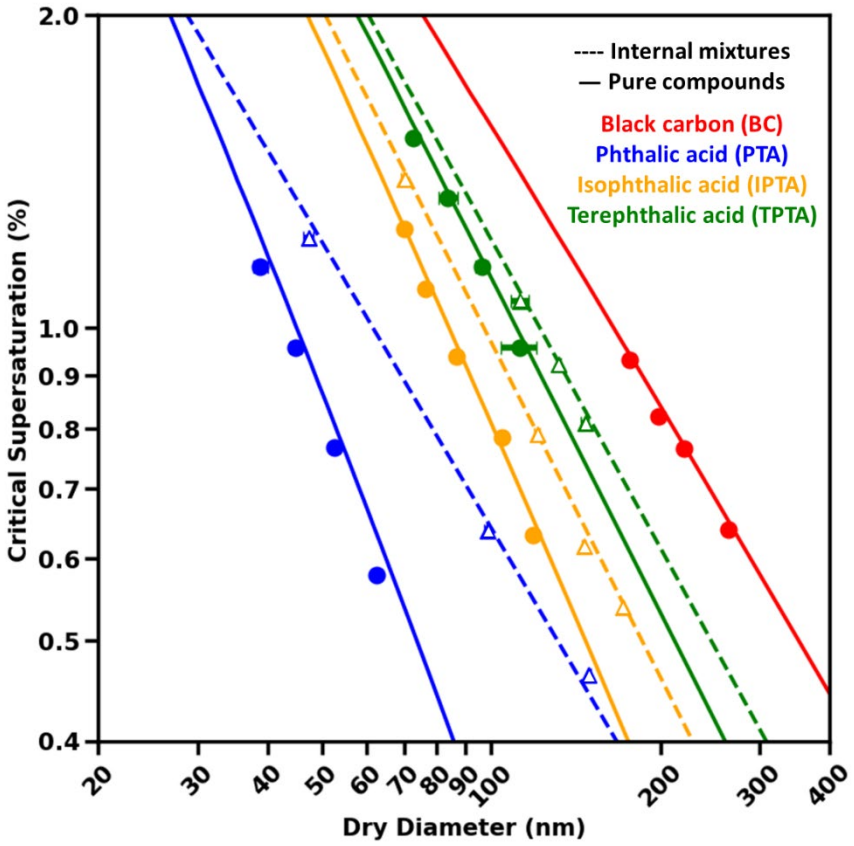

Fig. 5. D_{dry} vs. S_c pairs derived from CCN measurements of pure single component (solid circles) and mixed BC (open triangles) aerosol is shown. The CCN measurements of the single component AAA samples (from Gohil et al. 2022) are also plotted. The FHH-AT fits are depicted using solid and dashed lines for pure and mixed samples, respectively. The particle dry diameter refers to the calculated volume equivalent diameters.

The changing slope of S_c vs. D_{dry} of the BC mixtures with respect to their corresponding pure AAA can be used to understand the relative importance of the mixture components on the overall CCN activity of the mixture in consideration. The FHH-AT fits at smaller particle sizes for each mixture converge towards the FHH-AT fits of the corresponding pure AAA. This implies that the CCN activity of the given BC mixture is predominantly affected by the AAA present in the mixture, i.e., the particle morphology and composition of a BC mixture is affected by the corresponding AAA at smaller D_{ve}. Analogously, the morphology, composition, and CCN activity of the mixture particles is affected by BC at larger D_{ve}, due to the diverging FHH-AT fits.

Along with FHH-AT, the application of HAM was also studied for the pure and mixed BC aerosol (Fig. 6). For the CCN activity analysis with HAM, the aqueous solubility of BC was assumed to be 10^{-6} g/g water. Similar to FHH-AT, HAM fittings for pure and mixed BC aerosol were also compared to those for pure AAAs. Generally, the FHH-AT and HAM generate similar CCN activity predictions for pure and mixed BC aerosol under either of the BC aqueous solubility assumption. The R^2 goodness of fit scores (summarized in Table 2) for mixed aerosol all marginally increase for HAM; this is likely due to the explicit treatment of the AAA mixed with BC. However, there are subtle differences between the CCN activity predictions of FHH-AT and HAM for pure BC ($R^2_{FHH} = 0.957$ vs. $R^2_{HAM} = 0.899$). These differences could be due to the explicit treatment of aqueous solubility of BC in the HAM framework. FHH-AT fundamentally assumes the particles to be completely water insoluble and therefore the FHH-AT CCN activity predictions are independent of the water solubility of the compounds. A non-zero assumed solubility (10^{-6} g/g water) of pure BC results in a slight underprediction of CCN activity with HAM as compared to FHH-AT.

Table 2. FHH empirical parameters and R^2 scores for pure and mixed aerosol.

Sample	A^{c}_{FHH}	B^{c}_{FHH}	R^{2}_{FHH}	R^{2}_{HAM}
Black Carbon (Vulcan® XC72R)	7.54	2.26	0.957	0.899
Phthalic acid (PTA)	0.41	0.76	0.892	0.986
Isophthalic acid (IPTA)	0.39	0.87	0.936	0.967
Terephthalic acid (TPTA)	0.16	0.84	0.944	0.989
1:1 PTA-to-BC	1.37	1.11	0.875	0.991
1:1 IPTA-to-BC	0.23	0.87	0.908	0.954
1:1 TPTA-to-BC	0.27	1.04	0.934	0.943

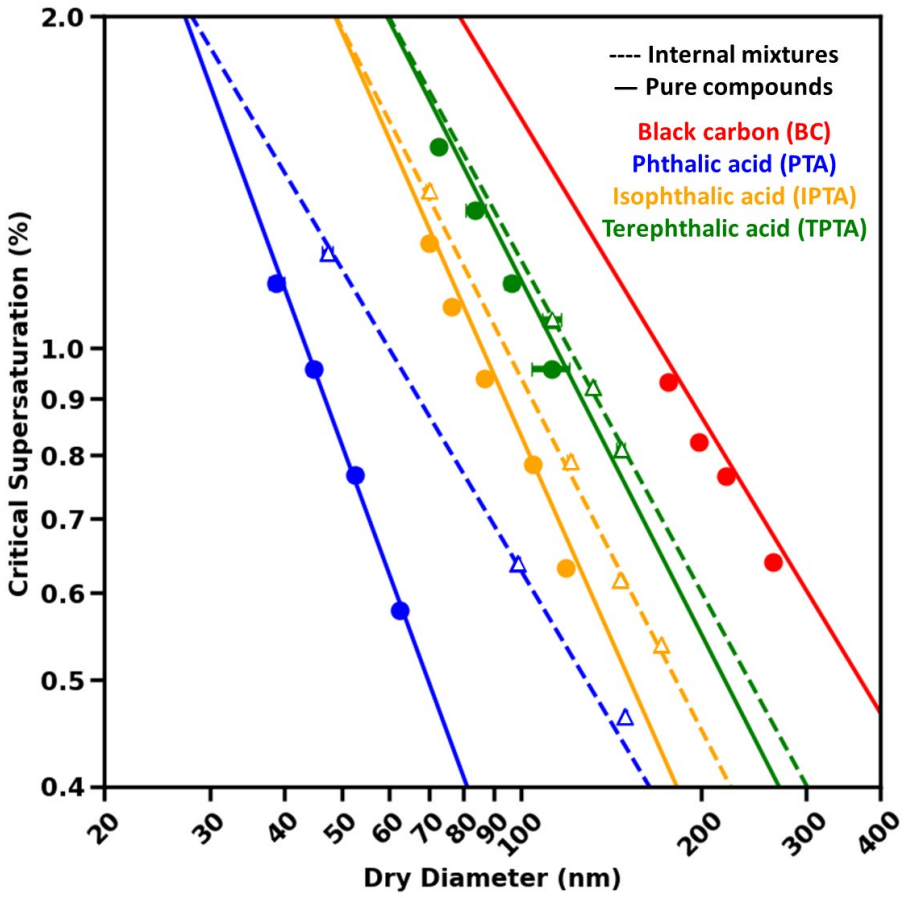

Fig. 6. D_{dry} vs. S_c pairs derived using the CCN measurements are shown as in Fig. 5. HAM fits for pure and mixed BC are depicted as solid and dashed lines, respectively. The HAM fits for pure

AAA are also shown as solid lines using the same colors as their corresponding mixture with BC. The HAM fits for all 7 sets of $D_{dry} - S_c$ pairs used the FHH empirical parameters determined by fitting FHH-AT across the measured data (Table 2) and are the same set of empirical parameters that were used to fit FHH-AT fitting in Fig. 5.

The hygroscopicity of the pure and mixed BC aerosol was also parameterized from HAM (κ_{HAM}) and compared to the κ_{HAM} of pure AAAs (Fig. 7). It was noted that κ_{HAM} of mixed BC aerosol declined sharply compared to κ_{HAM} values of the corresponding pure AAA. This sharp decline in the hygroscopicity of the mixture can be attributed to an increased influence of BC on the overall water uptake behavior of the BC mixtures. Moreover, κ_{HAM} of BC mixtures are especially low compared to the κ_{HAM} of the corresponding pure AAA at larger D_{dry}. These disparities in the κ_{HAM} at larger sizes between BC mixtures and their corresponding AAAs further suggests a strong influence of BC on the overall CCN activity of the larger sized mixture particles. As with the S_c vs D_{dry} data, subtle underestimations can be observed in the size-resolved BC κ_{HAM}. These slight underprediction is also associated with the explicit implementation of BC solubility (10^{-6} g/g water) in the κ_{HAM} parameterization.

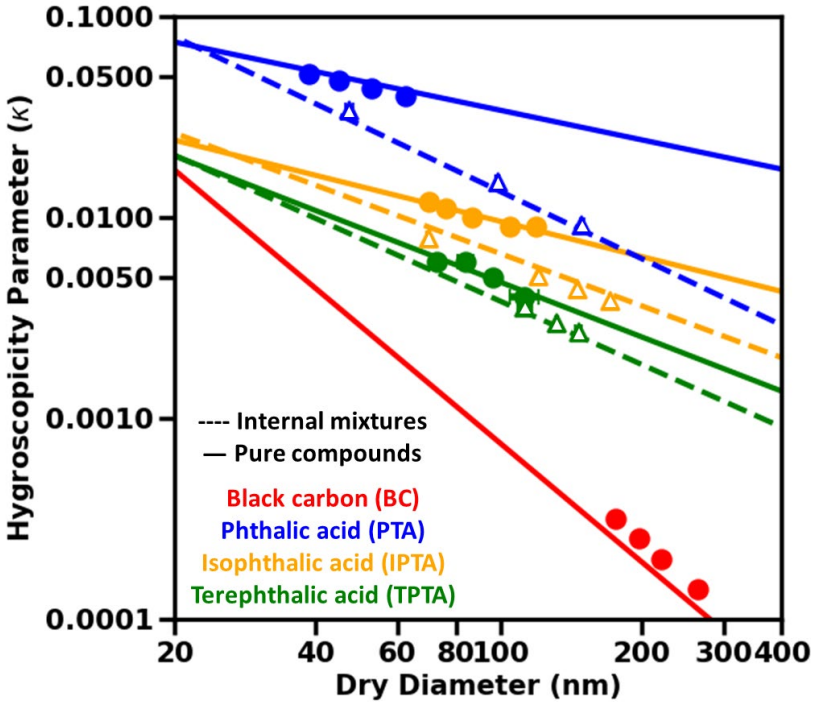

Fig. 7. Hygroscopicity parameterization from HAM (κ_{HAM}) is shown for pure (closed circles) and mixed BC with pure AAAs (open triangles). The individual points correspond to κ_{HAM} parameterized using experimental data, and the fitted curves correspond to the D_{dry}-dependent theoretical (or, simplified) κ_{HAM} as described in Gohil et al. (2022). The size-dependent decrease in the hygroscopicity of BC-PTA is much more prominent than that in the hygroscopicity of BC-IPTA and BC-TPTA as compared to their pure AAA counterparts.

Conclusions and discussion

This work presents the analysis of the water uptake of pure black carbon (BC) and BC mixed with low-water solubility organic compounds. Because BC is known to show changes in mixing state across size distributions, CCN measurements were performed for constant size particles selected in stepping mode. However, at a constant particle size, TEM and CCN analysis suggested that the mixtures presented here had components of carbon and oxidized species uniformly

distributed throughout the particles. Therefore, BC mixtures in this work were treated as internal mixtures implying that BC with other carbonaceous aerosol has the propensity to form homogenous internal mixtures.

The dynamic shape factor and effective density were also estimated for pure and mixed BC aerosol with respect to electrical mobility diameters. For all aerosol, the effective density was found to increase, and the shape factor was found to decrease with respect to size. It was inferred that these size-resolved trends were a consequence of the agglomeration of BC particles. It is to be noted that the TEM of BC mixtures also show that larger particles are more spherical than the smaller ones. However, TEM of the pure BC particles suggest that smaller particles are more compact and spherical compared to particles with larger volume equivalent diameters that exist as agglomerated fractal-like structures. Further examination of changes in particle shape and density is needed to understand the possible causes for large deviations from sphericity at smaller sizes for pure BC particles.

The CCN activity analysis of the pure and internally mixed (or, homogenous) BC was performed using the FHH-AT and HAM frameworks. FHH-AT is a widely known CCN activity model that describes water uptake through adsorption of water on particle surface. HAM is a recently developed framework that combines the FHH isotherm with the dissolved fraction of the particle accounting for the solubility limit of the compound. An explicit treatment of the solubility becomes significant for compounds that are sparingly soluble or effectively insoluble in water, and therefore HAM is particularly useful for the CCN analysis of such compounds. The utility of HAM is notable through its application to the experimental CCN data of pure and mixed BC aerosol. The CCN activity for internal mixtures predicted using HAM is comparable to that predicted using FHH-AT (Table 2, R^2 scores for BC internal mixtures). The CCN activity prediction of pure BC using HAM

is only marginally different than that predicted using FHH-AT on account for a finite water solubility consideration for BC in HAM (Table 2, R^2 scores for pure BC). Since there is no significant difference between FHH-AT and HAM predictions, HAM should be generally used for CCN analysis since HAM explicitly accounts for the effect of the bulk aqueous solubility on the overall water uptake behavior of any given chemical species.

Overall, HAM has utility for the CCN analysis of low-water solubility species such as BC and can also predict the size-dependent single hygroscopicity parameter. The CCN activities of BC mixed particles were mainly affected by AAA at smaller particle size. The impact of water-insoluble BC aerosol becomes pronounced at larger aerosol sizes. Indeed, mixed particles of smaller size have a greater perceived hygroscopicity than larger sized particles. Water adsorption, (FHH theory) is diameter dependent whereas traditional full dissolution theories (e.g, Köhler theory) are not. Indeed, traditional full dissolution assumptions should not be applied to aerosol solute that exhibit size-dependent hygroscopicity. In particular, droplet growth and hygroscopicity models for BC aerosol mixtures should be applied judiciously, and depending on the aerosol composition may require adsorption mechanisms, dissolution mechanisms, or both. HAM was first developed for the CCN activity analysis and hygroscopicity parameterization of the atmospherically relevant aerosols that possess low water solubility. However, HAM is ambidextrous and can also be applied to soluble inorganic and organics and mixtures when the process of solute dissolution dominates. With highly soluble mixtures, the effects of adsorption become negligible, and the size dependent droplet growth is not observed. It should also be noted that the phase of mixtures can modify water uptake and previous papers have measured the impact of viscosity, solute diffusivity, and crystallinity to account for impacts to droplet growth [70–73].

HAM does not explicitly account for phase, rather it accounts for the presence (or lack thereof) of an adsorptive surface (likely due to aerosol phase).

Previously, HAM had been applied in controlled laboratory measurements of specific organic compounds with aqueous solubility varying over a range of 2-3 orders of magnitude. This work expands upon the applicability of HAM for BC species observed in the atmosphere using agglomerated pure and mixed BC particles as a proxy. It should be noted that the oxygen to carbon ratio in of the BC mixtures was kept constant however the overall solute solubility was varied with the three AAAs. From here on, HAM can potentially be used for CCN activity analysis and hygroscopicity parameterization of other inorganic and organic species. This is valuable because HAM may be used for representing the hygroscopicity of organic and inorganic aerosol modes in Global Climate Models (GCMs), henceforth potentially improving the forcing due to aerosol indirect effect.

Associated Content

The following files are available free of charge.

Exemplary CCNC supersaturation calibration data used in this work; raw CCNC activation data for pure and mixed BC species (PDF)

Author Information

Corresponding Author

Akua Asa-Awuku – Department of Chemical and Biomolecular Engineering, University of Maryland, CollegePark, Maryland 20742, United States; https://orcid.org/0000-0002-0354-8368; Email: asaawuku@umd.edu

Author

Kanishk Gohil – Department of Chemical and Biomolecular Engineering, University of Maryland, College Park, Maryland 20742, United States; https://orcid.org/0000-0001-8500-9888

Author Contributions

KG and RB collected the CCN activity data for all samples. RB collected the shape factor and effective density data for all samples. DR collected and analyzed the TEM data for all samples.

KG and CNM developed the hybrid activity model and hygroscopicity parameterization. KG conducted CCN activity analysis across the datasets and prepared the manuscript with input from all co-authors. QY was instrumental in the acquisition of Vulcan samples, and initial testing of the black carbon material. All authors contributed to the development of the study and writing of the manuscript. All authors have given approval to the final version of the manuscript.

Funding

This research work was funded by the National Science Foundation (NSF grant# 2003927).

Notes

The authors declare no competing interests.

Acknowledgments

The authors acknowledge the support for this research by graduate awards in the Department of Chemical and Biomolecular Engineering (University of Maryland) and the National Science Foundation.

References

(1) Arden Pope, C.; Dockery, D. W. Epidemiology of Particle Effects. In *Air Pollution and Health*; Elsevier, 1999; pp 673–705. https://doi.org/10.1016/B978-012352335-8/50106-X.

(2) Highwood, E. J.; Kinnersley, R. P. When Smoke Gets in Our Eyes: The Multiple Impacts of Atmospheric Black Carbon on Climate, Air Quality and Health. *Environ Int* **2006**, *32* (4), 560–566. https://doi.org/10.1016/j.envint.2005.12.003.

(3) Ramanathan, V.; Carmichael, G. Global and Regional Climate Changes Due to Black Carbon. *Nat Geosci* **2008**, *1* (4), 221–227. https://doi.org/10.1038/ngeo156.

(4) Crutzen, P. J.; Andreae, M. O. Biomass Burning in the Tropics: Impact on Atmospheric Chemistry and Biogeochemical Cycles. *Science (1979)* **1990**, *250* (4988), 1669–1678. https://doi.org/10.1126/science.250.4988.1669.

(5) Vermote, E.; Ellicott, E.; Dubovik, O.; Lapyonok, T.; Chin, M.; Giglio, L.; Roberts, G. J. An Approach to Estimate Global Biomass Burning Emissions of Organic and Black Carbon from MODIS Fire Radiative Power. *J Geophys Res* **2009**, *114* (D18), D18205. https://doi.org/10.1029/2008JD011188.

(6) Intergovernmental Panel on Climate Change. Working Group 1 Science; Intergovernmental Panel on Climate Change; Intergovernmental Panel on Climate Change. Working Group I. *Climate Change 2007 - The Physical Science Basis: Working Group Contribution to the Fourth Assessment Report of the IPCC*; Cambridge University Press, 2007.

(7) Bond, T. C.; Doherty, S. J.; Fahey, D. W.; Forster, P. M.; Berntsen, T.; DeAngelo, B. J.; Flanner, M. G.; Ghan, S.; Kärcher, B.; Koch, D.; et al. Bounding the Role of Black Carbon in the Climate System: A Scientific Assessment. *J Geophys Res: Atmospheres* **2013**, *118* (11), 5380–5552. https://doi.org/10.1002/jgrd.50171.

(8) Weingartner, E.; Burtscher, H.; Baltensperger, U. Hygroscopic Properties of Carbon and Diesel Soot Particles. *Atmos Environ* **1997**, *31* (15), 2311–2327. https://doi.org/10.1016/S1352-2310(97)00023-X.

(9) Zhang, R.; Khalizov, A. F.; Pagels, J.; Zhang, D.; Xue, H.; McMurry, P. H. Variability in Morphology, Hygroscopicity, and Optical Properties of Soot Aerosols during Atmospheric Processing. *PNAS* **2008**, *105* (30), 10291–10296. https://doi.org/10.1073/pnas.0804860105.

(10) Laaksonen, A.; Malila, J.; Nenes, A. Heterogeneous Nucleation of Water Vapor on Different Types of Black Carbon Particles. *Atmos Chem Phys* **2020**, *20* (21), 13579–13589. https://doi.org/10.5194/acp-20-13579-2020.

(11) Canagaratna, M. R.; Jimenez, J. L.; Kroll, J. H.; Chen, Q.; Kessler, S. H.; Massoli, P.; Hildebrandt Ruiz, L.; Fortner, E.; Williams, L. R.; Wilson, K. R.; et al. Elemental Ratio Measurements of Organic Compounds Using Aerosol Mass Spectrometry: Characterization, Improved Calibration, and Implications. *Atmos Chem Phys* **2015**, *15* (1), 253–272. https://doi.org/10.5194/acp-15-253-2015.

(12) Zhang, S.; Wang, M.; Ghan, S. J.; Ding, A.; Wang, H.; Zhang, K.; Neubauer, D.; Lohmann, U.; Ferrachat, S.; Takeamura, T.; et al. On the Characteristics of Aerosol Indirect Effect Based on Dynamic Regimes in Global Climate Models. *Atmos Chem Phys* **2016**, *16* (5), 2765–2783. https://doi.org/10.5194/acp-16-2765-2016.

(13) Peng, J.; Hu, M.; Guo, S.; Du, Z.; Zheng, J.; Shang, D.; Levy Zamora, M.; Zeng, L.; Shao, M.; Wu, Y.-S.; et al. Markedly Enhanced Absorption and Direct Radiative Forcing of Black Carbon under Polluted Urban Environments. *PNAS* **2016**, *113* (16), 4266–4271. https://doi.org/10.1073/pnas.1602310113.

(14) Dusek, U.; Reischl, G. P.; Hitzenberger, R. CCN Activation of Pure and Coated Carbon Black Particles. *Environ Sci Technol* **2006**, *40* (4), 1223–1230. https://doi.org/10.1021/es0503478.

(15) Stratmann, F.; Bilde, M.; Dusek, U.; Frank, G. P.; Hennig, T.; Henning, S.; Kiendler-Scharr, A.; Kiselev, A.; Kristensson, A.; Lieberwirth, I.; et al. Examination of Laboratory-Generated Coated Soot Particles: An Overview of the LACIS Experiment in November (LExNo) Campaign. *J Geophys Res* **2010**, *115* (D11), D11203. https://doi.org/10.1029/2009JD012628.

(16) Maskey, S.; Chong, K. Y.; Seo, A.; Park, M.; Lee, K.; Park, K. Cloud Condensation Nuclei Activation of Internally Mixed Black Carbon Particles. *Aerosol Air Qual Res* **2017**, *17* (4), 867–877. https://doi.org/10.4209/aaqr.2016.06.0229.

(17) Dalirian, M.; Ylisirniä, A.; Buchholz, A.; Schlesinger, D.; others. Cloud Droplet Activation of Black Carbon Particles Coated with Organic Compounds of Varying Solubility. **2018**.

(18) Laaksonen, A.; Malila, J.; Nenes, A.; Hung, H.-M.; Chen, J.-P. Surface Fractal Dimension, Water Adsorption Efficiency and Cloud Nucleation Activity of Insoluble Aerosol. *Sci Rep* **2016**, *6* (1), 25504. https://doi.org/10.1038/srep25504.

(19) Laaksonen, A.; Malila, J.; Nenes, A. Heterogeneous Nucleation of Water Vapor on Different Types of Black Carbon Particles. *Atmos Chem Phys* **2020**, *20* (21), 13579–13589. https://doi.org/10.5194/acp-20-13579-2020.

(20) Sorjamaa, R.; Laaksonen, A. The Effect of H_2O Adsorption on Cloud Drop Activation of Insoluble Particles: A Theoretical Framework. *Atmos Chem Phys* **2007**, *7* (24), 6175–6180. https://doi.org/10.5194/acp-7-6175-2007.

(21) Kumar, P.; Sokolik, I. N.; Nenes, A. Parameterization of Cloud Droplet Formation for Global and Regional Models: Including Adsorption Activation from Insoluble CCN. *Atmos Chem Phys* **2009**, *9* (7), 2517–2532. https://doi.org/10.5194/acp-9-2517-2009.

(22) Kumar, P.; Nenes, A.; Sokolik, I. N. Importance of Adsorption for CCN Activity and Hygroscopic of Mineral Dust Aerosol. *Geophys. Res. Lett.* **2009**.

(23) Kumar, P.; Sokolik, I. N.; Nenes, A. Measurements of Cloud Condensation Nuclei Activity and Droplet Kinetics of Fresh Unprocessed Regional Dust samples and Minerals. *Atmos. Chem. Phys.* **2011**.

(24) Kumar, P.; Sokolik, I. N.; Nenes, A. Cloud Condensation Nuclei Activity and Droplet Activation of Wet Processed Regional Dust Samples and Minerals. *Atmos. Chem. Phys.* **2011**.

(25) Hatch, C. D.; Wiese, J. S.; Crane, C. C.; Harris, K. J.; Kloss, H. G.; Baltrusaitis, J. Water Adsorption on Clay Minerals as a Function of Relative Humidity: Application of BET and Freundlich Adsorption Models. *Langmuir* **2012**, *28* (3), 1790–1803. https://doi.org/10.1021/la2042873.

(26) Hatch, C. D.; Greenaway, A. L.; Christie, M. J.; Baltrusaitis, J. Water Adsorption Constrained Frenkel–Halsey–Hill Adsorption Activation Theory: Montmorillonite and Illite. *Atmos Environ* **2014**, *87*, 26–33. https://doi.org/10.1016/j.atmosenv.2013.12.040.

(27) Hatch, C. D.; Tumminello, P. R.; Cassingham Megan A and Greenaway, A. L.; Meredith, R.; Christie, M. J. Technical Note: Frenkel, Halsey and Hill Analysis of Water on Clay: Toward Closure between Cloud Condensation Nuclei and Water Adsorption. *Atmos. Chem. Phys*. 2019, pp 13581–13589.

(28) Tang, M.; Cziczo, D. J.; Grassian, V. H. Interactions of Water with Mineral Dust Aerosol: Water Adsorption, Hygroscopicity, Cloud Condensation, and Ice Nucleation. *Chem Rev* **2016**, *116* (7), 4205–4259. https://doi.org/10.1021/acs.chemrev.5b00529.

(29) Kuwata, M.; Kondo, Y.; Takegawa, N. Critical Condensed Mass for Activation of Black Carbon as Cloud Condensation Nuclei in Tokyo. *J Geophys Res* **2009**, *114* (D20), D20202. https://doi.org/10.1029/2009JD012086.

(30) Novakov, T.; Corrigan, C. E. Cloud Condensation Nucleus Activity of the Organic Component of Biomass Smoke Particles. *Geophys Res Lett* **1996**, *23* (16), 2141–2144. https://doi.org/10.1029/96GL01971.

(31) Vu, D.; Gao, S.; Berte, T.; Kacarab, M.; others. External and Internal Cloud Condensation Nuclei (CCN) Mixtures: Controlled Laboratory Studies of Varying Mixing States. *Atmospheric* **2019**.

(32) FURUTANI, H.; DALLOSTO, M.; ROBERTS, G.; PRATHER, K. Assessment of the Relative Importance of Atmospheric Aging on CCN Activity Derived from Field Observations. *Atmos Environ* **2008**, *42* (13), 3130–3142. https://doi.org/10.1016/j.atmosenv.2007.09.024.

(33) M.J. Lázaro; L. Calvillo; v. Celorrio; J.I. Pardo; S. Perathoner; R. Moliner. *Study And Application of Carbon Black Vulcan Xc-72r In Polymeric Electrolyte Fuel Cells*; Sanders, I. J., Peeten, T. L., Eds.; Nova Science Publishers, Inc., 2011.

(34) Fu, P.; Kawamura, K.; Barrie, L. A. Photochemical and Other Sources of Organic Compounds in the Canadian High Arctic Aerosol Pollution during Winter−Spring. *Environ Sci Technol* **2009**, *43* (2), 286–292. https://doi.org/10.1021/es803046q.

(35) Singh, D. K.; Kawamura, K.; Yanase, A.; Barrie, L. A. Distributions of Polycyclic Aromatic Hydrocarbons, Aromatic Ketones, Carboxylic Acids, and Trace Metals in Arctic Aerosols:

Long-Range Atmospheric Transport, Photochemical Degradation/Production at Polar Sunrise. *Environ Sci Technol* **2017**, *51* (16), 8992–9004. https://doi.org/10.1021/acs.est.7b01644.

(36) Meng, J.; Wang, G.; Hou, Z.; Liu, X.; Wei, B.; Wu, C.; Cao, C.; Wang, J.; Li, J.; Cao, J.; et al. Molecular Distribution and Stable Carbon Isotopic Compositions of Dicarboxylic Acids and Related SOA from Biogenic Sources in the Summertime Atmosphere of Mt. Tai in the North China Plain. *Atmos Chem Phys* **2018**, *18* (20), 15069–15086. https://doi.org/10.5194/acp-18-15069-2018.

(37) Haque, Md. M.; Kawamura, K.; Deshmukh, D. K.; Fang, C.; Song, W.; Mengying, B.; Zhang, Y.-L. Characterization of Organic Aerosols from a Chinese Megacity during Winter: Predominance of Fossil Fuel Combustion. *Atmos Chem Phys* **2019**, *19* (7), 5147–5164. https://doi.org/10.5194/acp-19-5147-2019.

(38) Kunwar, B.; Kawamura, K.; Fujiwara, S.; Fu, P.; Miyazaki, Y.; Pokhrel, A. Dicarboxylic Acids, Oxocarboxylic Acids and α-Dicarbonyls in Atmospheric Aerosols from Mt. Fuji, Japan: Implication for Primary Emission versus Secondary Formation. *Atmos Res* **2019**, *221*, 58–71. https://doi.org/10.1016/j.atmosres.2019.01.021.

(39) Liu, H.; Kawamura, K.; Kunwar, B.; Cao, J.; Zhang, J.; Zhan, C.; Zheng, J.; Yao, R.; Liu, T.; Xiao, W. Dicarboxylic Acids and Related Compounds in Fine Particulate Matter Aerosols in Huangshi, Central China. *J Air Waste Manage Assoc* **2019**, *69* (4), 513–526. https://doi.org/10.1080/10962247.2018.1557089.

(40) Yassine, M. M.; Suski, M.; Dabek-Zlotorzynska, E. Characterization of Benzene Polycarboxylic Acids and Polar Nitroaromatic Compounds in Atmospheric Aerosols Using UPLC-MS/MS. *J Chromatogr A* **2020**, *1630*, 461507. https://doi.org/10.1016/j.chroma.2020.461507.

(41) Kanellopoulos, P. G.; Verouti, E.; Chrysochou, E.; Koukoulakis, K.; Bakeas, E. Primary and Secondary Organic Aerosol in an Urban/Industrial Site: Sources, Health Implications and the Role of Plastic Enriched Waste Burning. *J Environ Sci* **2021**, *99*, 222–238. https://doi.org/10.1016/j.jes.2020.06.012.

(42) Mkoma, S. L.; Kawamura, K. Molecular Composition of Dicarboxylic Acids, Ketocarboxylic Acids, α-Dicarbonyls and Fatty Acids in Atmospheric Aerosols from Tanzania, East Africa during Wet and Dry Seasons. *Atmos Chem Phys* **2013**, *13* (4), 2235–2251. https://doi.org/10.5194/acp-13-2235-2013.

(43) Balla, D.; Voutsa, D.; Samara, C. Study of Polar Organic Compounds in Airborne Particulate Matter of a Coastal Urban City. *Environmental Science and Pollution Research* **2018**, *25* (13), 12191–12205. https://doi.org/10.1007/s11356-017-9993-2.

(44) Al-Naiema, I. M.; Stone, E. A. Evaluation of Anthropogenic Secondary Organic Aerosol Tracers from Aromatic Hydrocarbons. *Atmos Chem Phys* **2017**, *17* (3), 2053–2065. https://doi.org/10.5194/acp-17-2053-2017.

(45) Zhong, X.; Cui, C.; Yu, S. Exploring the Pathways of Aromatic Carboxylic Acids in Ozone Solutions. *RSC Adv* **2017**, *7* (55), 34339–34347. https://doi.org/10.1039/C7RA03039H.

(46) Zhong, X.; Cui, C.; Yu, S. The Determination and Fate of Disinfection By-Products from Ozonation-Chlorination of Fulvic Acid. *Environmental Science and Pollution Research* **2017**, *24* (7), 6472–6480. https://doi.org/10.1007/s11356-016-8350-1.

(47) Kleindienst, T. E.; Jaoui, M.; Lewandowski, M.; Offenberg, J. H.; Docherty, K. S. The Formation of SOA and Chemical Tracer Compounds from the Photooxidation of Naphthalene and Its Methyl Analogs in the Presence and Absence of Nitrogen Oxides. *Atmos Chem Phys* **2012**, *12* (18), 8711–8726. https://doi.org/10.5194/acp-12-8711-2012.

(48) He, X.; Huang, X. H. H.; Chow, K. S.; Wang, Q.; Zhang, T.; Wu, D.; Yu, J. Z. Abundance and Sources of Phthalic Acids, Benzene-Tricarboxylic Acids, and Phenolic Acids in PM $_{2.5}$ at Urban and Suburban Sites in Southern China. *ACS Earth Space Chem* **2018**, *2* (2), 147–158. https://doi.org/10.1021/acsearthspacechem.7b00131.

(49) Al-Naiema, I. M.; Offenberg, J. H.; Madler, C. J.; Lewandowski, M.; Kettler, J.; Fang, T.; Stone, E. A. Secondary Organic Aerosols from Aromatic Hydrocarbons and Their Contribution to Fine Particulate Matter in Atlanta, Georgia. *Atmos Environ* **2020**, *223*, 117227. https://doi.org/10.1016/j.atmosenv.2019.117227.

(50) Gohil, K.; Mao, C.-N.; Rastogi, D.; Peng, C.; Tang, M.; Asa-Awuku, A. Hybrid Water Adsorption and Solubility Partitioning for Aerosol Hygroscopicity and Droplet Growth. *Atmos Chem Phys* **2022**, *22* (19), 12769–12787. https://doi.org/10.5194/acp-22-12769-2022.

(51) Mahajan, O. P.; Moreno-castilla, C.; Walker, P. L. Surface-Treated Activated Carbon for Removal of Phenol from Water. *Sep Sci Technol* **1980**, *15* (10), 1733–1752. https://doi.org/10.1080/01496398008055619.

(52) Das, N. C.; Khastgir, D.; Chaki, T. K.; Chakraborty, A. Electromagnetic Interference Shielding Effectiveness of Carbon Black and Carbon Fibre Filled EVA and NR Based Composites. *Compos Part A Appl Sci Manuf* **2000**, *31* (10), 1069–1081. https://doi.org/10.1016/S1359-835X(00)00064-6.

(53) Assumpção, M. H. M. T.; De Souza, R. F. B.; Rascio, D. C.; Silva, J. C. M.; Calegaro, M. L.; Gaubeur, I.; Paixão, T. R. L. C.; Hammer, P.; Lanza, M. R. V.; Santos, M. C. A Comparative Study of the Electrogeneration of Hydrogen Peroxide Using Vulcan and Printex Carbon Supports. *Carbon N Y* **2011**, *49* (8), 2842–2851. https://doi.org/10.1016/j.carbon.2011.03.014.

(54) Tang, S.; Sun, G.; Qi, J.; Sun, S.; Guo, J.; Xin, Q.; Haarberg, G. M. Review of New Carbon Materials as Catalyst Supports in Direct Alcohol Fuel Cells. *Chinese Journal of Catalysis* **2010**, *31* (1), 12–17. https://doi.org/10.1016/S1872-2067(09)60034-6.

(55) Carmo, M.; dos Santos, A. R.; Poco, J. G. R.; Linardi, M. Physical and Electrochemical Evaluation of Commercial Carbon Black as Electrocatalysts Supports for DMFC

Applications. *J Power Sources* **2007**, *173* (2), 860–866. https://doi.org/10.1016/j.jpowsour.2007.08.032.

(56) Kinoshita, K.; Bett, J. A. S. Potentiodynamic Analysis of Surface Oxides on Carbon Blacks. *Carbon N Y* **1973**, *11* (4), 403–411. https://doi.org/10.1016/0008-6223(73)90080-8.

(57) Wagner, S.; Ding, Y.; Jaffé, R. A New Perspective on the Apparent Solubility of Dissolved Black Carbon. *Front Earth Sci (Lausanne)* **2017**, *5*. https://doi.org/10.3389/feart.2017.00075.

(58) Roberts, G. C.; Nenes, A. A Continuous-Flow Streamwise Thermal-Gradient CCN Chamber for Atmospheric Measurements. *Aerosol Sci. Technol.* **2005**, *39* (3), 206–221. https://doi.org/10.1080/027868290913988.

(59) Engelhart, G. J.; Asa-Awuku, A.; Nenes, A.; Pandis, S. N. CCN Activity and Droplet Growth Kinetics of Fresh and Aged Secondary Organic Aerosol. **2008**. *Atmos Chem Phys* 8: 3937-3949.

(60) Moore, R. H.; Nenes, A.; Medina, J. Scanning Mobility CCN Analysis—A Method for Fast of Size-Resolved CCN Distributions and Activation Kinetics. *Aerosol Sci. Technol.* **2010**, *44* (10), 861–871.

(61) Barati, F.; Yao, Q.; Asa-Awuku, A. A. Insight into the Role of Water-Soluble Organic Solvents for the Cloud Condensation Nuclei Activation of Cholesterol. *ACS Earth Space Chem.* **2019**, *3* (9), 1697–1705.

(62) Tavakoli, F.; Symonds, J. P. R.; Olfert, J. S. Generation of a Monodisperse Size-Classified Aerosol Independent of Particle Charge. *Aerosol Sci. Technol.* **2014**, *48* (3), i–iv. https://doi.org/10.1080/02786826.2013.877121.

(63) Tavakoli, F.; Olfert, J. S. Determination of Particle Mass, Effective Density, Mass–Mobility, and Dynamic Shape Factor Using an Aerodynamic Aerosol and a Differential Mobility Analyzer in Tandem. *J. Aerosol Sci.* **2014**, *75*, 35–42.

(64) Yao, Q.; Asa-Awuku, A.; Zangmeister, C. D.; Radney, J. G. Comparison of Three Essential Sub-Micrometer Aerosol: Mass, Size and Shape. *Aerosol Sci. Technol.* **2020**, *54* (10), 1197–1209.

(65) Gohil, K.; Asa-Awuku, A. A. Cloud Condensation Nuclei (CCN) Activity Analysis of Low-Hygroscopicity Aerosols Using the Aerodynamic Aerosol Classifier (AAC). *Aerosol Measurement Techniques* **2022**, *15* (4), 1007–1019.

(66) Niemi, K.; Baumann, M. H.; Kovanen, P. T.; Eklund, K. K. Serum Amyloid A (SAA) Activates Human Mast Cells Which Leads into Degradation of SAA and Generation of an Amyloidogenic SAA Fragment. *Biochimica et Biophysica Acta (BBA) - Molecular Basis of Disease* **2006**, *1762* (4), 424–430. https://doi.org/10.1016/j.bbadis.2006.01.001.

(67) Rastogi, D.; Asa-Awuku, A. Size, Shape, and Phase of Nanoscale Uric Acid Particles. *ACS Omega* **2022**, *7* (28), 24202–24207. https://doi.org/10.1021/acsomega.2c01213.

(68) Riipinen, I.; Rastak, N.; Pandis, S. N. Connecting the Solubility and CCN Activation of Complex Organic Aerosols: A Theoretical Study Using Solubility Distributions. *Atmos Chem Phys* **2015**, *15* (11), 6305–6322. https://doi.org/10.5194/acp-15-6305-2015.

(69) Petters, M. D.; Kreidenweis, S. M. A Single Parameter Representation of Hygroscopic Growth and Cloud Condensation Nucleus Activity. *Atmos Chem Phys* **2007**, *7* (8), 1961–1971. https://doi.org/10.5194/acp-7-1961-2007.

(70) Peng, B.; Wu, R.; Li, H. Crystallization from a Droplet: Single-Crystalline Arrays and Heterojunctions for Organic Electronics. *Acc Chem Res* **2021**, *54* (24), 4498–4507. https://doi.org/10.1021/acs.accounts.1c00537.

(71) Wang, Z.; Orejon, D.; Sefiane, K.; Takata, Y. Water Vapor Uptake into Hygroscopic Lithium Bromide Desiccant Droplets: Mechanisms of Droplet Growth and Spreading. *Physical Chemistry Chemical Physics* **2019**, *21* (3), 1046–1058. https://doi.org/10.1039/C8CP04504F.

(72) Asa-Awuku, A.; Nenes, A. Effect of Solute Dissolution Kinetics on Cloud Droplet Formation: Extended Köhler Theory. *J Geophys Res* **2007**, *112* (D22), D22201. https://doi.org/10.1029/2005JD006934.

(73) Hings, S. S.; Wrobel, W. C.; Cross, E. S.; Worsnop, D. R.; Davidovits, P.; Onasch, T. B. CCN Activation Experiments with Adipic Acid: Effect of Particle Phase and Adipic Acid Coatings on Soluble and Insoluble Particles. *Atmos Chem Phys* **2008**, *8* (14), 3735–3748. https://doi.org/10.5194/acp-8-3735-2008.

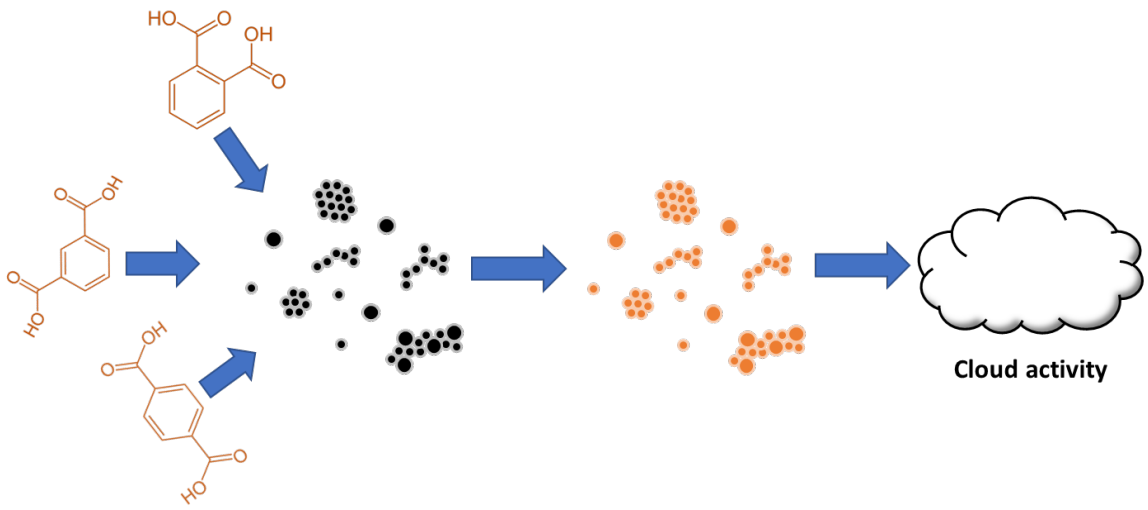

TOC Graphic